LINKÖPING UNIVERSITY

Thickness and Orientation dependent surface roughness and internal defect characterization of SLM Ti-6Al-4V

Final Bachelor Thesis

Student:

Agustín Monzón Vivas

LiU-IEI-TEK-G–20/01848-SE

17/06/2020

Contents

Page

List of Figures

List of Tables

1 Introduction

Manufacturing products using a powder bed fusion process is a brand new technique for industries which let them produce more complex geometries requiring far less initial material. But this new manufacturing process generates microstructures different from other observed in any manufacturing process since powder is melted one layer at a time by a laser beam. As a consequence, its mechanical properties have to be analyzed, thus, a previous research concludes that some of tested samples had poor mechanical properties which shall be examined.

Thus, a study of samples defects is required since it will point out why that poor mechanical properties are found and how it could be solved for prospective studies. This study will be focus on specific kind of surface defects such as surface roughness and how it is affecting to the geometry and it also will be focus on specific internal defects such lack of fusion and entrapped gas bubbles which will generate pores inside the sample. Those pores might be the main reason samples with poor fatigue life appears since it is a critical parameter for crack propagation, specially under fatigue stress.

Finally, the aim of this research is to characterize internal defects as well as external defects such as porosity quantification and surface roughness in order to get an idea of why there are some samples that have poor fatigue live and how it can be compensated or even get a solution for forthcoming researches.

2 Literature Review

3D-metal printing is a laser based manufacturing process using metal powder or metal wire. This first method consist on a metal powder bed which is melted by a laser beam one layer at a time; once the layer is done, a new metal powder layer cover that previous layer in order to provide more material to the laser beam. While in the wire based method, a similar way as 3D-plastic printing is used where the difference is that for metal wire, a laser beam is used so that the metal can be melted. Those manufacturing method let engineers to create quick prototypes of complex geometries such cooling ducts inside the geometry or even some complex medical prosthesis, so they can be tested unlike 3D plastic printed prototypes. But not everything is good news in this business. Lots of parameters must be controlled in order to create a proper geometry such as the building direction, laser beam speed, laser hatch angle, type of powder and so on [5] [6].

2.1 Direct Metal Laser Sintering (DMLS)

The DMLS process is a Powder Based Fusion (PBF) process which means that a powder bed is used instead of wire form. In order to make this process happen, two tanks of metal powder are used. The first tank is where all the metal powder is storage which is used to fill the second one, in where the laser beam is melting the metal powder; one layer at a time as seen in figure 2.1. When a layer is done, the first tank fills the second one with another metal powder layer and this process is repeated until the solid is done. This process is taking part into an inert environment made out of argon gas which is used in order to prevent oxidation, corrosion and maintaining constant pressure so that a stable printing environment is created. As well as DMLS process, some other ways of metal printing are used as main PBF process such as Selective Laser Sintering (SLS)/Selective Laser Melting (SLM) and Electron Beam Melting (EBM) [7].

Although this technique has several advantages, it also has some important disadvantages such as lack of fusion which let some unmelted powder inside the part, porosity and a high surface roughness. All of this defects generates crack starters which make the part livelong less than it should be [8].

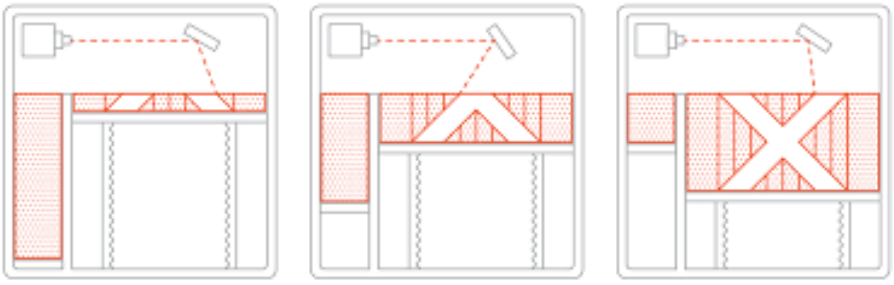

Figure 2.1: Schematic DMLS process

2.1.1 Influence of building direction in mechanical properties

As it is known, mechanical properties of a solid usually depends on the manufacturing process since this is the main reason imperfections such pores or crack starters appear. One of those influence factors in this 3D-metal printing is the building direction which could be crucial for some properties and it is define as the angle between the longest axis of the fabricated sample and the horizontal plane [9]. As it is covered in the article [1] for steel 316L samples, some specimens where tested in different building orientations (figure 2.2 [1]) giving some important conclusions about how this parameter could affect the sample. Those samples tested at vertical directions had higher tensile strength as well as average elongation than those tested at vertical direction. Then, it was found the worst elongation and strength combination for those samples tested at 0 degrees, while those samples tested at 45 degrees had the best strength and ductility combination. Although in the article [10], for steel 304 samples, the worst tensile properties were found.

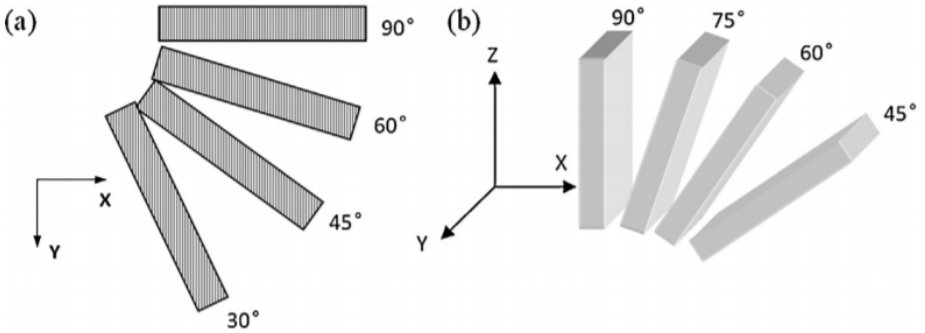

Figure 2.2: Building orientation for fatigue specimen [1].

Those differences between samples tested in those different articles are related to grain orientation and how it is formed depending on the solidification phase parameters which is explain in the article [11].

2.2 Fatigue

Fatigue life is subjected to stress cycles in where stress fluctuates, commonly, as fully reversed loading as seen in the top graphic from figure 2.3, from a lower value which has a same absolute value as it maximum stress value getting an average stress value equal to 0. This cycle is used in testing and it is almost the same cycle a rotating axis may meet during service. Another typical cycle is the one show in the middle of this same figure which its highest stress value, as well as the lower one is above 0 (tensile) although it can also be under 0 (compression). Besides this, it is not a condition both of them have an equal absolute value. Finally, the last type of stress cycle is random or spectrum load (last graphic from figure 2.3) which a random load is applied over the cycle.

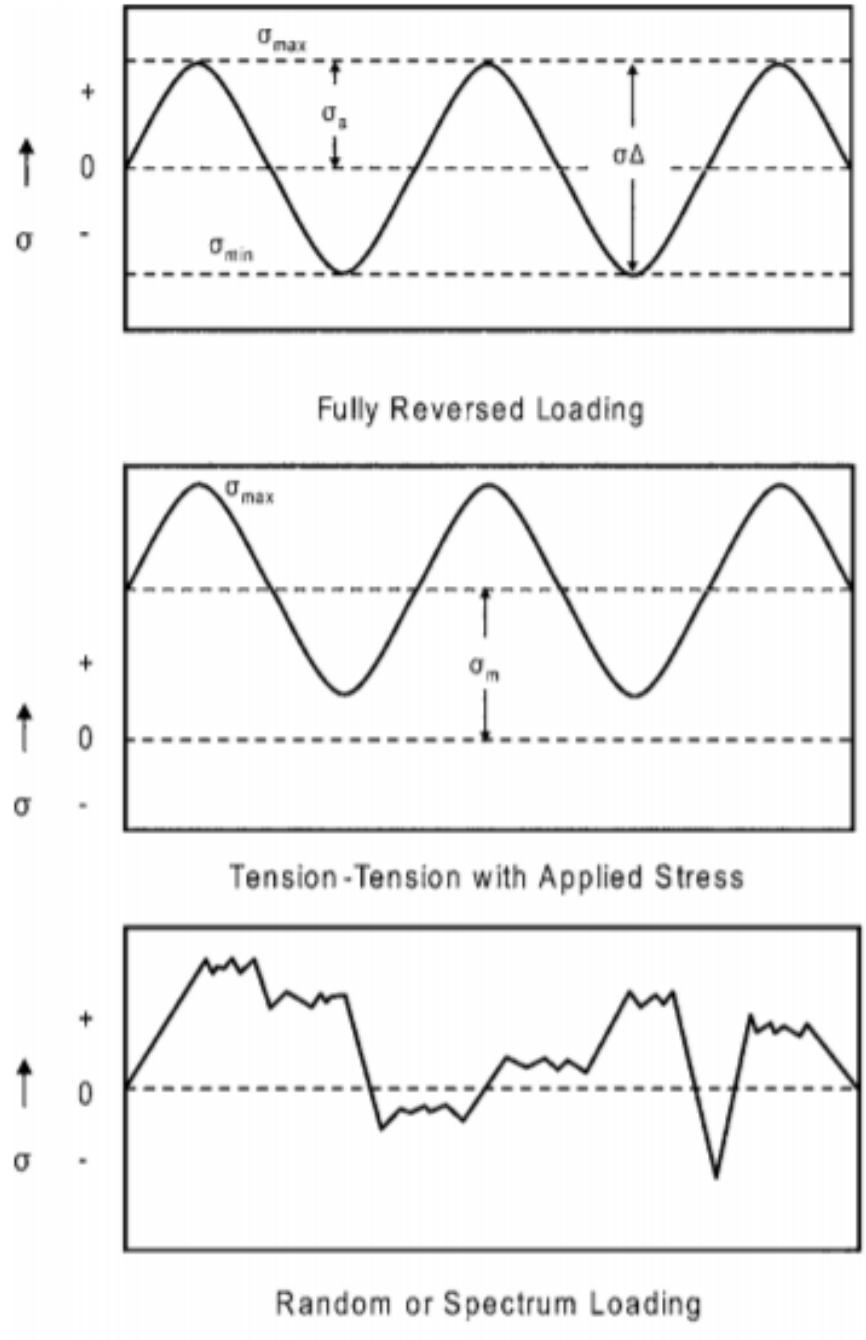

Figure 2.3: Schematic of fatigue loading cycles [2].

Those components from fluctuating stress are mean stress, σ_m, alternating stress σ_a and stress range, σ_r which are represented in equations below.

$$\sigma_r = \sigma_{max} - \sigma_{min}$$

$$\sigma_a = \frac{\sigma_r}{2} = \frac{\sigma_{max} - \sigma_{min}}{2}$$

$$\sigma_m = \frac{\sigma_{max} + \sigma_{min}}{2}$$

Then, fatigue failure is the crack obtained applying a high variation of stress over a cycle, a high stress value on the maximum stress of the cycle or enough cycle to make the part collapse. For this kind of failure, three different stages as seen in figure 2.4 can be observed: nucleation, crack growth and final failure. Due to stress variations, creep damage appear in this first stage (nucleation) although the maximum stress of the cycle is low compared to its yield stress. Here, some microscopic cracks appear in surface discontinuities which, as the same time it appears, it is also being polished or even melted again because of the back-and-forth movement of the part. This phenomena is called formation of persistent slip bands. Those cracks show up first in fragile materials since there is no creep for this kind of materials. Then, once the crack length has grown enough to become critical for stress field, second stages begins. In this stage, crack propagation, striations over the fracture surface are created which each one represents one cycle from the fatigue failure. Finally, once the remaining cross-section due to the crack formed is too low, it breaks since it can no longer support the load applied and this is the final stage, final failure [2].

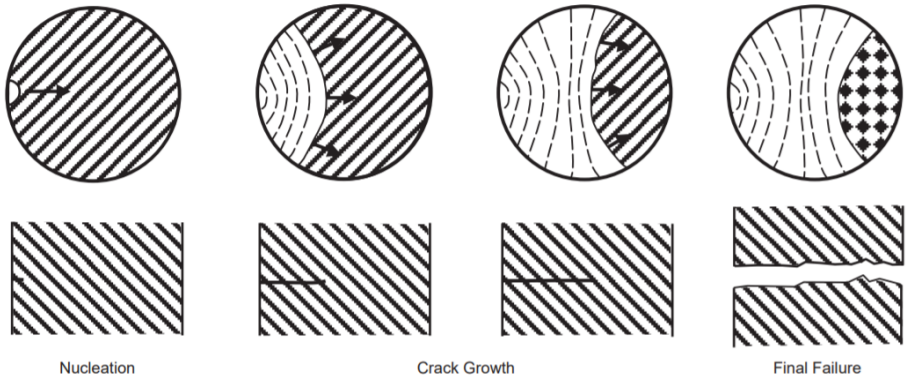

Figure 2.4: Fatigue crack propagation [2].

2.3 Porosity due to DMLS

Porosity is a common defect in additive manufacturing process, so several studies have been done on this topic. This defect can appear because of over melting or lack of melting and it makes the part weak reducing its mechanical properties. Some studies [4] show that the higher the laser scan speed is, the higher the porosity formation due to lack of energy density is. Besides this, a high laser energy density generates entrapped gas bubbles which forms spherical pores since that thermal energy is conducted downwards melting a deep zone which, in case the part has some geometry holes, can melt the bottom layer allowing gas bubbles going upwards. Then, a high solidification rate do not let enough time for bubbles to escape, generating pores which can be measured. However, this porosity formation increase non-linearly to the energy density although it is also dependent on laser beam focus, which is one of "lack of fusion" defect generator. This overlapping and defocusing (figure 2.5) effect let some powder between laser beam tracks which wont be melted and it will end up in that lack of fusion pores formation (figure 2.6).

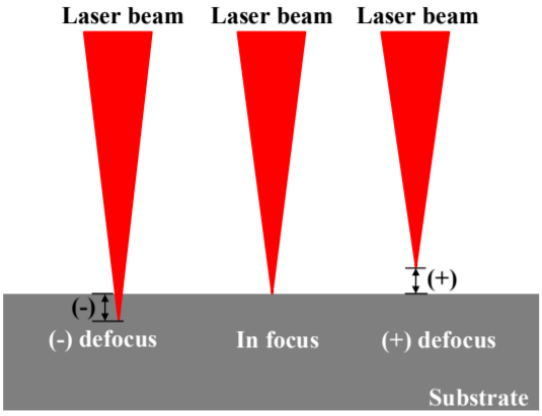

Figure 2.5: Schematic of defocusing distance [3]

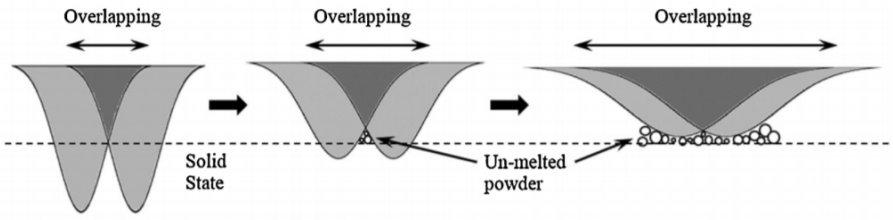

Figure 2.6: Schematic of melting pool with increase focus offset [4]

Powder size as well as powder morphology also influence in pores formation defect [3]. As it is shown, small and spherical powder is the optimal one in order to reach the least pore formation since those spheres will reflect the laser ray in such a way that a uniform melted pool is reached as seen in figure 2.7 where small and spherical powder is the first one, then, non-spherical particles are seen in second place and picture c and d are a mix of them [8].

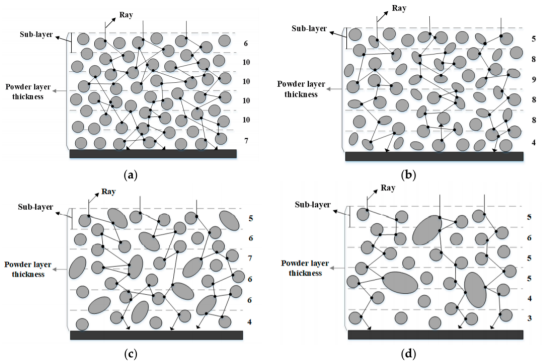

Figure 2.7: Illustration of RT model [3]

3 Previous Work

In this sections a short summary about what has been done in the previous research is given. The aim of that research was to investigate Ti-6Al-4V components properties for aeronautical application while a 3D-printing manufacturing method is used. In order to fulfill that objective, samples in Ti-6Al-4V have been manufactured using two different manufacturing method: Selective Laser Melting (SLM) and Electron Laser Melting (ELM). Then, after some research, it was found that, depending on how samples are 3D-printed, its mechanical properties are not the same. This phenomena specially occurs on fatigue properties which is one of the most important properties for this project since fatigue failure is one of the most common failure in aeronautical applications.

Then, samples were manufactured in three different orientations: 0 degrees, 45 degrees and 90 degrees relative to the build plate as well as three different thicknesses from 1.3 to 2.5 millimeters according to figure 3.1. Although those samples are used for tensile and fatigue testing, both SLM ones and ELM ones got their geometry form ASTM E466. But some samples, which were fatigue tested, got a heat treatment according to ASTM F2924/F3001 2012 in order to improve its fatigue properties.

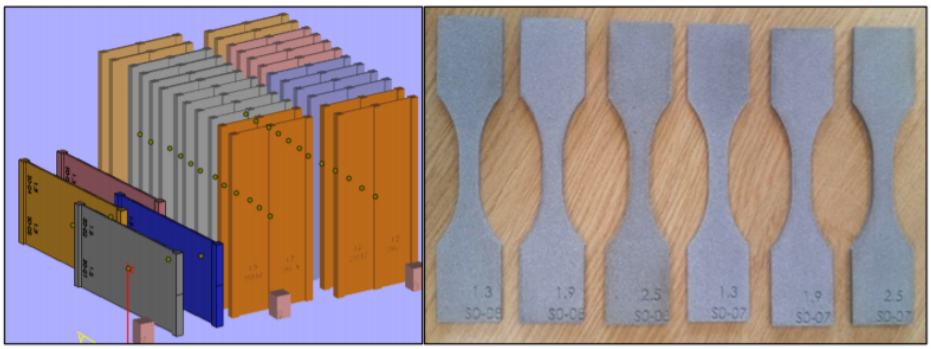

Figure 3.1: Specimen geometry and building orientation schema

Fatigue test were performed using constant amplitude and a load frequency of 10Hz. In order to cover a big range, from 50.000 cycles to 5.000.000 cycles to failure, stress amplitude were change between samples. Then, those samples which endure 5.000.000 cycles were consider as infinite fatigue live and were used again in test with a different stress amplitude so as to the maximum amount of data is obtained.While tensile testing was performed fulfilling ISO 6892-1 and it also was monitored in order to detect any anisotropic behaviour.

Graphics bellow (figures 3.2-3.4) show fatigue test results in where a scatter is observed which is provoked by samples which have a poor fatigue life braking before it should be. This phenomena is specially strong in samples built at 90 degrees in where a trend line is hard to visualize. However, a fatigue life trend line has been drawn for that graphic while this trend line is not necessary for both other graphics. In this work, that phenomena aforesaid is analyzed by looking at each sample's fracture surface since there can be observed a significant amount

of defect for those samples which had a poor fatigue life.

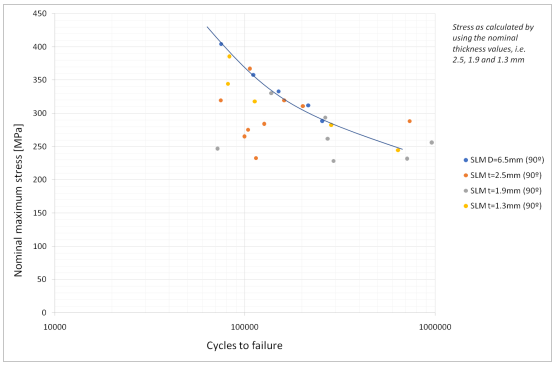

Figure 3.2: Fatigue live graphic for samples built at 90 degrees

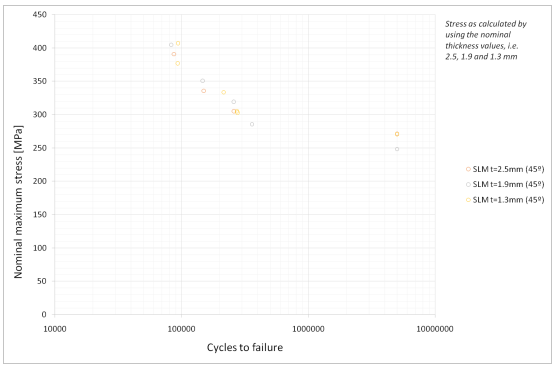

Figure 3.3: Fatigue live graphic for samples built at 45 degrees

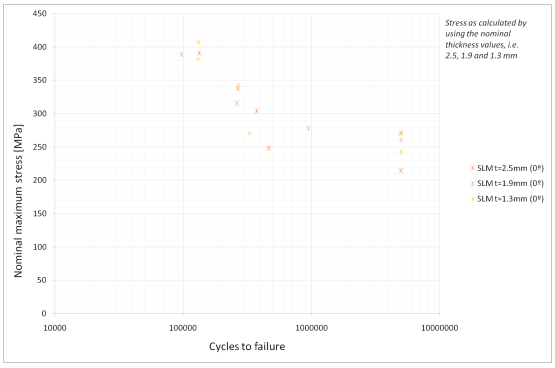

Figure 3.4: Fatigue live graphic for samples built at 0 degrees

Finally, some conclusion were reached. To begin with, a higher tensile strength, higher ductility as well as higher fatigue strength were fond for SLM material compared to EBM material, meaning SLM material reach better mechanical properties. Then, an explanation for that poor fatigue live aforesaid were found on internal defects such as pores and surface roughness due to a lack of fusion and a poor melting of particles in surface geometry. Besides this, samples built at 90 degrees are more sensitive to this failure as it can be seen on the amount of scatter those type of samples have from fatigue graphics and because of the load was apply along building directions. That is also the reason that research recommend not to built part along the direction the load is apply. In this study only the SLM samples will be considered for further evaluation.

4 Experimental method and results

4.1 Surface roughness

Surface roughness has been measured in order to get a compensation thickness factor so that it can be apply to data obtained from testing and get a correct stress value calculated using its true cross-section. Then, using a Surface Electron Microscope (SEM) surface roughness is measured taking images in z axis from the deepest hole until the highest peak as well as x-y plane along $20mm^2$ which are overlapped in order to get an accurate roughness measurement. Those images as seen in figures 4.1-4.3 which are obtained, where it can be observed a 3D image of the surface, are 3D-topography images which are going to be used in this compensation factor measurement.

Afterwards, using Leica Microsystems software, all roughness parameters has been obtained using a Gaussian filter in order to separate waviness from roughness. Then, a roughness profile for each sample is extracted in a perpendicular direction from its building direction in order to get an optimal measurement since, otherwise, a path between layers can be measured and it is not the real piece roughness. Two parameters has been selected from all the data extracted: average roughness (Ra) and roughness profile (Rt), which are used in the tables 4.1-4.3.

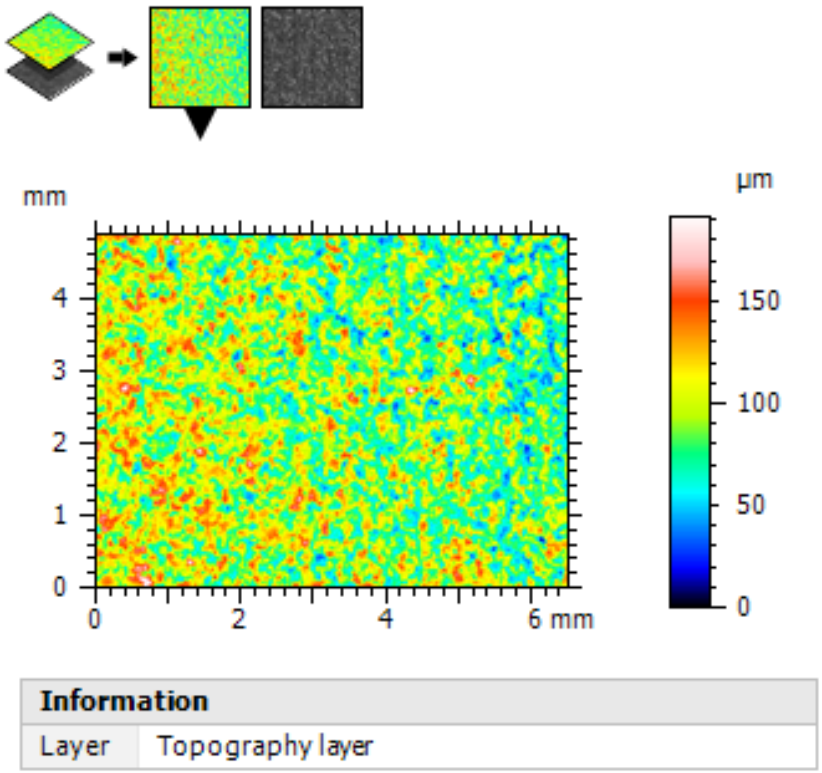

Figure 4.1: 1,3mm thickness surface roughness measurement using Surface Electron Microscope

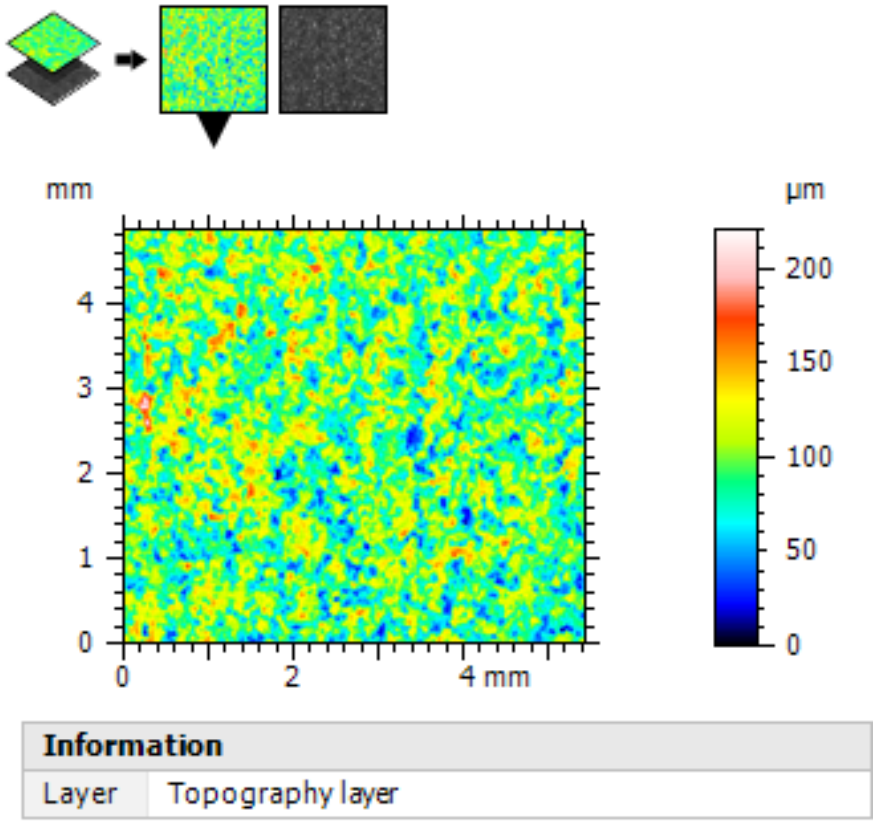

Figure 4.2: 1,9mm thickness surface roughness measurement using Surface Electron Microscope

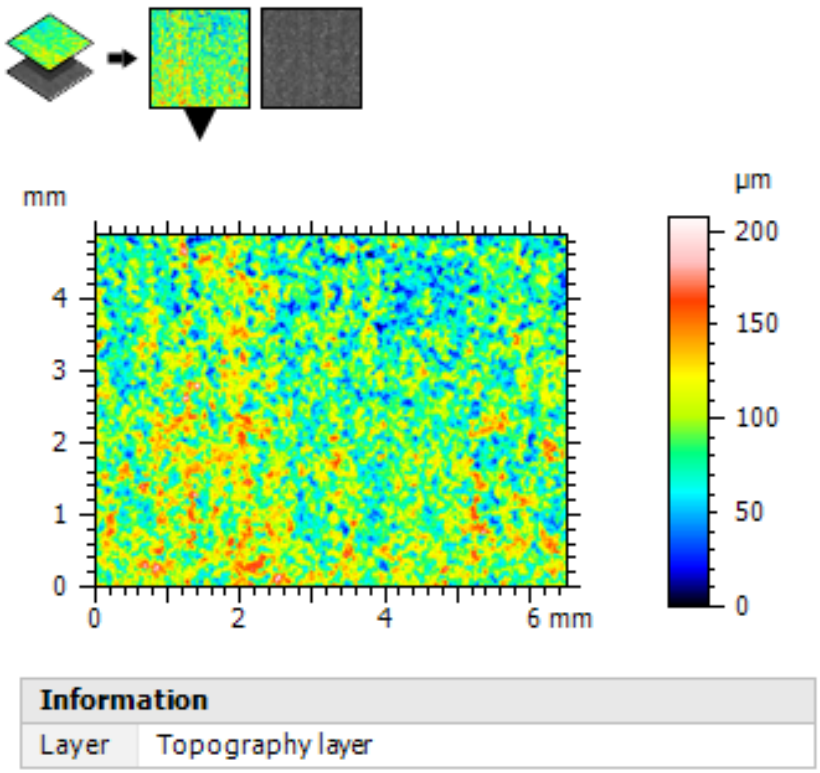

Figure 4.3: 2.5mm thickness surface roughness measurement using Surface Electron Microscope

Taking a look on tables 4.1-4.3 a clear roughness difference between those samples manufactured at 0 degrees, 45 degrees and 90 degrees is observed. The roughness average (Ra) value is 14.33 μm for samples manufactured at 0 degrees, 12.25 μm for samples manufactured at 45 degrees and 17.22 μm for samples manufactured at 90 degrees, giving a total average of 14.39 μm. While the total height of the roughness profile (Rt) is 97.60 μm for samples manufactured at 0 degrees, 81.04 μm for samples manufactured at 45 degrees and 123.56 μm for samples manufactured at 90 degrees, giving a total average of 97.60 μm.

Thus, looking at those values, a reduction of 47% is observed between samples built at 45 degrees (81.04 μm) and the current compensation factor value (150 μm), there is also a reduction of 40% between samples built at 0 degrees (92.08 μm) and the current compensation factor value and, finally, we can observe a reduction of 19% between samples built at 90 degrees (123.56μm) and the current compensation factor value. On this first look, it can be said that this compensation factor is a bit high.

	2.5 mm width											
	S0				S45			S90				
Ra (µm)	17.1	13.4	13.7	12.1	12.2	11.8	8.64	16.1	16.4	16.2	17.0	19.0
Rt (µm)	118.0	88.2	93.0	85.2	78.9	66.1	62.6	114.0	102.0	118.0	138.0	128.0

Table 4.1: Surface roughness for 2.5 mm width samples

	1.9 mm width										
	S0			S45				S90			
Ra (µm)	18.6	10.8	14.2	15.1	10.8	9.79	10.3	17.5	18.2	17.4	15.2
Rt (µm)	98.0	84.7	82.5	123.0	80.7	63.1	55.2	140.0	129.0	118.0	118.0

Table 4.2: Surface roughness for 1.9 mm width samples

	1.3 mm width										
	S0			S45				S90			
Ra (µm)	14.6	12.9	15.9	14.8	15.5	13.0	11.2	13.9	17.2	18.0	18.0
Rt (µm)	96.8	74.9	99.5	104.0	102.0	81.1	71.7	84.1	146.0	126.0	119.0

Table 4.3: Surface roughness for 1.3 mm width samples

4.2 Porosity

Several samples have unexpected low fatigue life and some defects are detected in the fracture surface. One of the most common defect in additive manufacturing techniques is a high porosity ratio. Thus, in order to get a general idea of the amount of defects our samples have, a porosity measurement is going to be done all over the sample. Once it is done, it can be known how many and where defects are located so we can achieve a conclusion of why those samples have that low fatigue life.

Porosity has been measured using three different techniques. Starting by Archimedes method, a scale density kit XPR-S XSR-S as seen in figure 4.4 is used which contains two different places to do measurements into a box which isolates the sample form dust and everything that could generate a mismeasurement. The first measurement is being carried out in a container full of a liquid which in this case distilled water is used with a thermometer into it so that water temperature can be known and, therefore, water density is known. Then, the sample weight is measured outside the water container and knowing water density, air density and both sample weights, sample density can be known using the equation shown below. Where A is the sample weight outside the water tank, B is the sample weight inside the water tank, ρ_0 is the liquid density and ρ_L is the air density. Both measurements are being done three times each part of the tested sample, so a total of six measurements are done in order to maximize the precision.

Figure 4.4: Density Kit XPR-S XSR-S 0.1mg, 1mg

$$\rho = \frac{A}{A-B} \cdot (\rho_0 - \rho_L) + \rho_L$$

Those values obtained using this method can be seen on tables 4.4, 4.5 and 4.6 where samples density has been measured using Archimedes method while samples porosity is the difference between theoretical Ti-6Al-4V alloy density and density which has been measured. Doing so, it can be known the amount of porosity which will be check using the fracture surface as well as a cross-section from samples which are the second and third porosity measurement methods respectively.

For this second method, an optical microscope has been used so that a better look on the fracture surface is taken. Once this image is recorded, it can be observed some defects all over this surface as we can appreciate in figure 4.5. But there are some other samples that do not have that obvious defects as figure 4.6. so that is the reason image's brightness has been lowered and image's contrast has been maximized giving as a result a picture like seen in figure 4.7 and figure 4.8 where defect are shining. Thus, we can get a better look on the fracture surface and a good analysis is going to be done since defects are easy to identify.

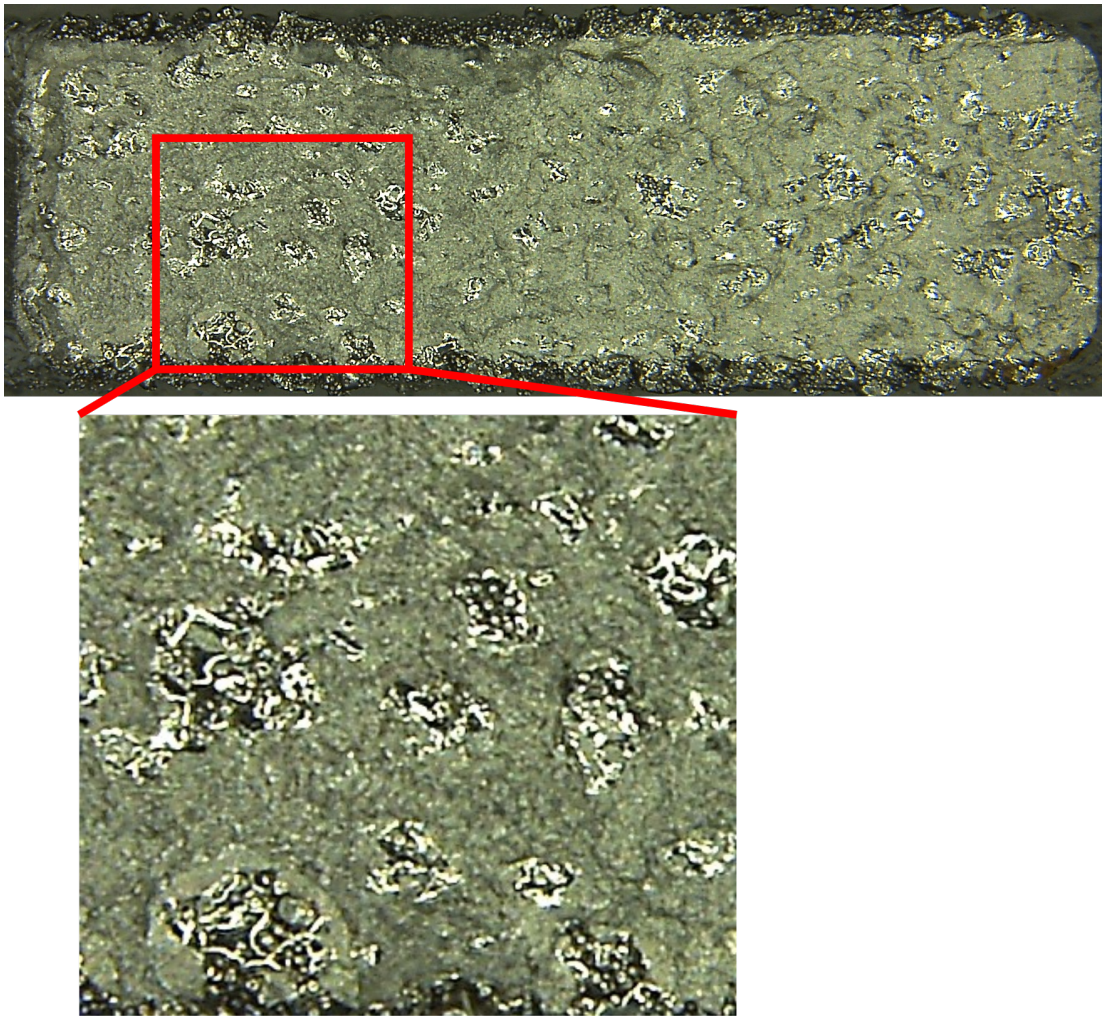

Figure 4.5: First example of an image taken using an optical microscope

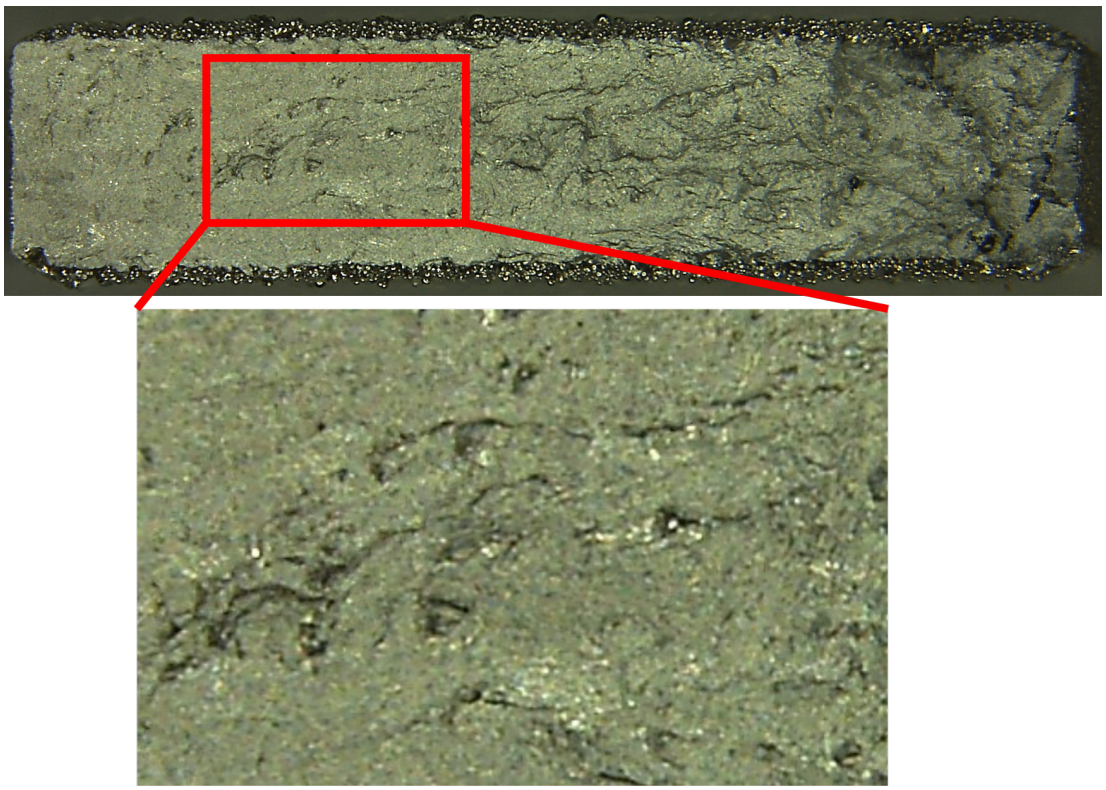

Figure 4.6: Second example of an image taken using an optical microscope

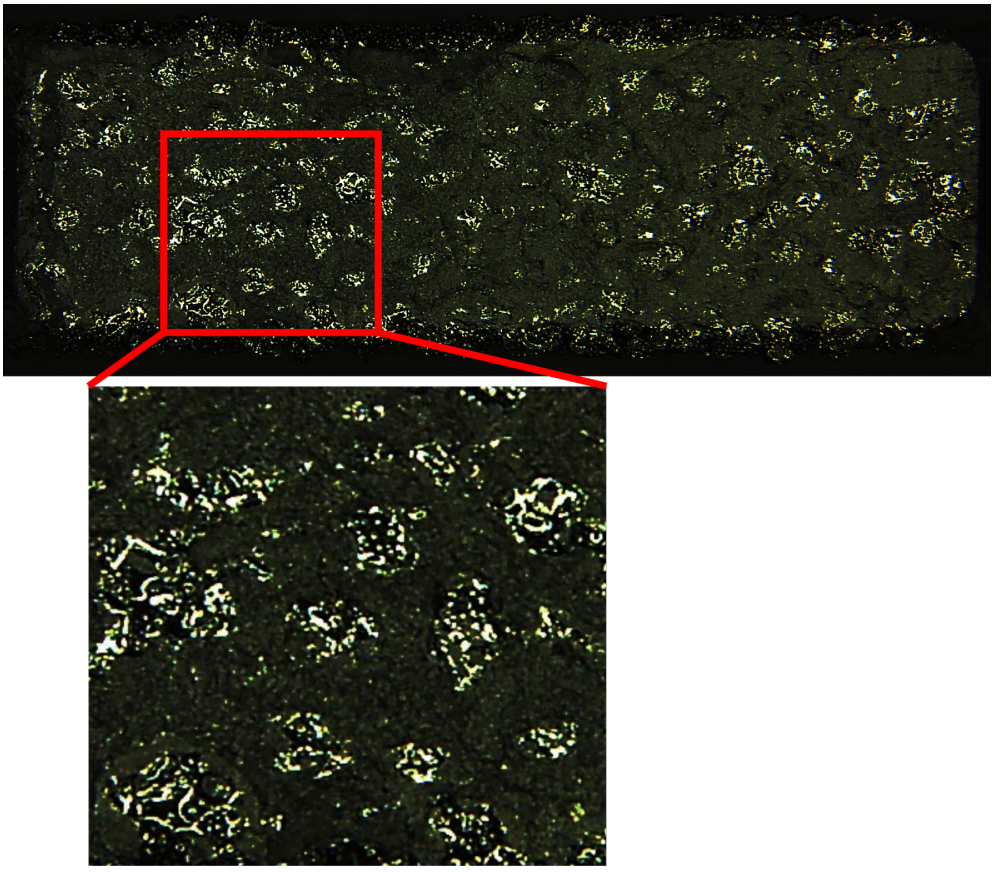

Figure 4.7: First example of a post processed image taken using an optical microscope

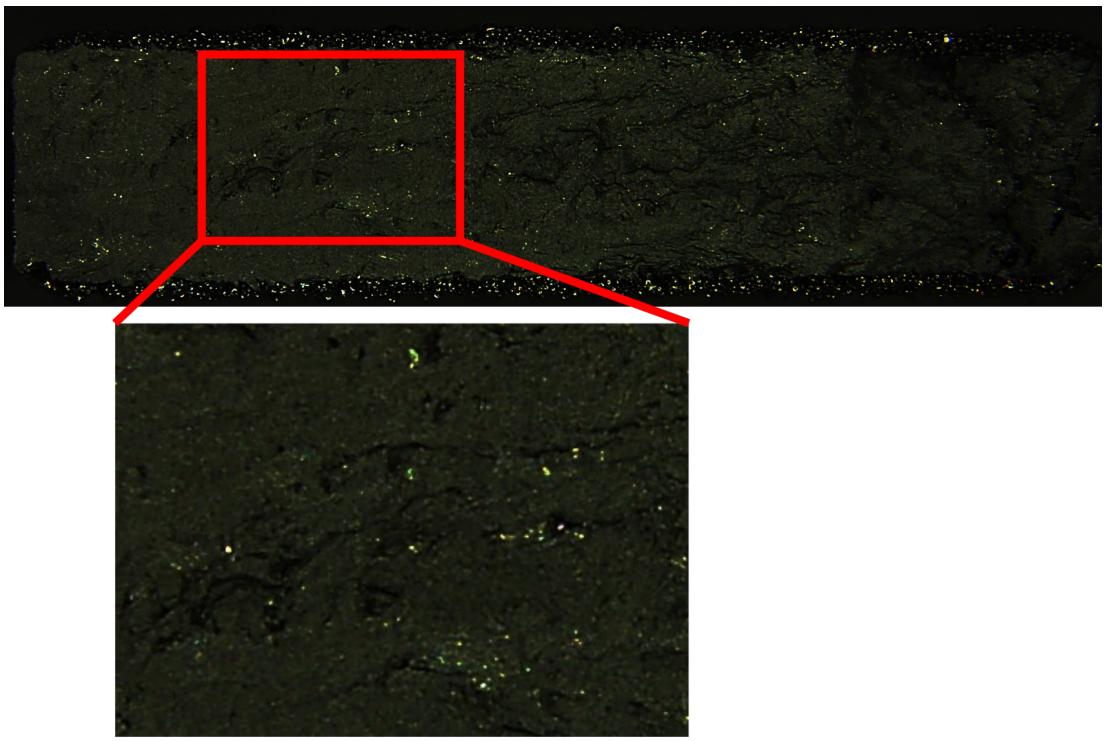

Figure 4.8: Second example of a post processed image taken using an optical microscope

Finally, for this third method, a destructive method cutting a small part of the sample has been performed in order to make a cross-section out of it. A first cut as it is shown as a red plane in figure 4.9 is done since this is what is going to be tested. This part is being mounted into a polymer sample for its following polish. In order to get a good sample cross-section, some millimeters are going to be removed before polishing. A cross-section plane as the blue plane in figure 4.9 is trying to be achieve so 1mm is going to be removed from 2.5mm thickness samples, 0.8mm is going to be removed from 1.9mm thickness samples and 0.5mm from 1.3mm thickness samples. Then, a six steps polishing is applied to those samples and an image as seen in figure 4.10 is obtained.

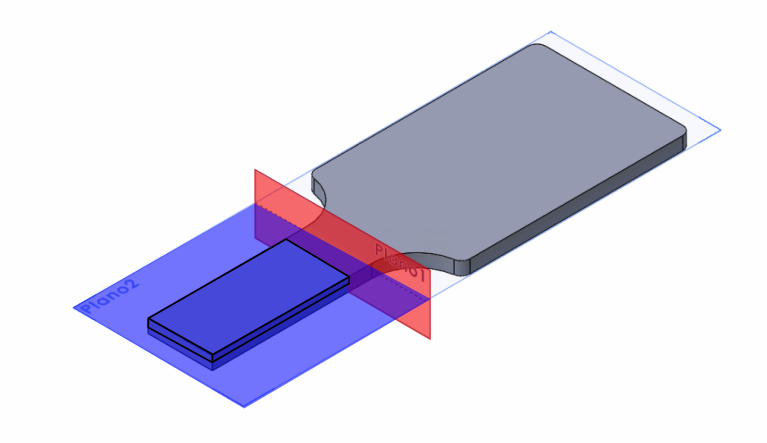

Figure 4.9: Cross-section schema

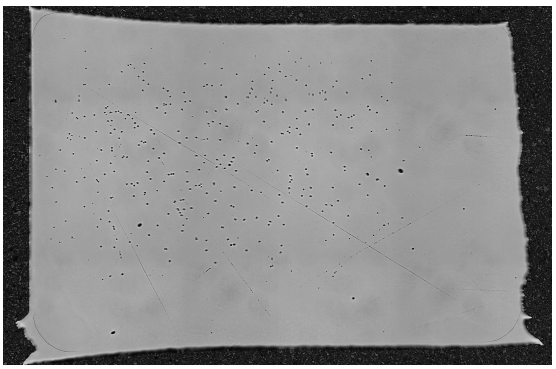

Figure 4.10: Example of a cross-section polished

Taking a look on tables 4.4-4.6 a clear porosity ratio difference between those samples built at 0 degrees, 45 degrees and 90 degrees is observed. Porosity ratio average value is 1.85% where for samples manufactured at 0 degrees is 1.25% which is pretty close to the percentile. Then, a porosity ratio of 0.95% is found for samples built at 45 degrees while a porosity ratio of 3.01% is found for samples built at 90 degrees. Moreover, as one can observe on roughness tables 4.1-4.3, some manufacturing failure are found for samples built at 90 degrees since those ones are the ones which has the most number of defects while samples built at 45 degrees are the ones which has the less number of defects. Then, observing fatigue life graphics from previous work chapter (figures 3.2-3.4) and comparing it to tables 4.4-4.6, one can observe that a porosity ratio of 1.70% is found for samples which are on fatigue life trend line as well as over it, being this value on the percentile. One can also observe that a porosity ratio of 2.39% is found for samples which are under fatigue life trend line, being this value higher than percentile value.

	2.5 mm width											
	S0				S45			S90				
Density (g/cm^3)	4.40	4.37	4.41	4.36	4.41	4.41	4.41	4.27	4.35	4.31	4.32	4.35
Porosity (%)	0.67	1.29	0.53	1.50	0.49	0.37	0.48	3.58	1.77	2.70	2.45	1.83

Table 4.4: Porosity measurement for 2.5 mm width samples

	1.9 mm width											
	S0			S45				S90				
Density (g/cm^3)	3.87	4.37	4.36	4.39	4.41	4.41	4.39	4.26	4.35	4.32	4.28	4.30
Porosity (%)	12.59	1.26	1.55	0.83	0.56	0.55	0.96	3.73	1.80	2.50	3.38	2.85

Table 4.5: Porosity measurement for 1.9 mm width samples

	1.3 mm width								
	S0				S45				
Density (g/cm^3)	4.33	4.38	4.39	4.40	4.33	4.34	4.41	4.41	4.35
Porosity (%)	2.33	1.15	0.84	0.59	2.36	1.93	0.49	0.55	1.87
			S90						
Density (g/cm^3)			4.19	4.30	4.24	4.31	4.29		
Porosity (%)			5.45	2.83	4.29	2.80	3.22		

Table 4.6: Porosity measurement for 1.3 mm width samples

Then, most represented samples from this scatter are being selected and its cross-sections has been done. Taking a look on all fatigue tested data as well as tables 4.4-4.6, where porosity data measured using Archimedes method is, most critical samples, those samples which are on the percentile and those ones which are under the percentile are selected for its cross-section evaluations. It would make sense that those samples which has more porosity rate, would also be under fatigue life trend line. However, there are some samples which has high porosity ratio as well as a high number of defects and those ones are also over fatigue life trend line. An example of it could be sample number ten built at 90 degrees with 2.5mm thickness which has a porosity ratio of 3.58% and it is over fatigue life trend line, where 1.85% is the average porosity ratio value and this one in particular is also over porosity ratio percentile for samples built at 90 degrees. Same thing happens also on the other way, there are some samples which has low porosity ratio as well as a high number of defects and those ones are also under fatigue life trend line. And an example of it could be sample number one built at 0 degrees with 2.5mm thickness which has a porosity ratio of 0.67% and it is under fatigue life trend line and it is also under porosity ratio percentile for samples built at 90 degrees. Thus, some of those samples are selected and analysed in figures 4.11-4.19.

Finally, fracture surface defects are compared to cross-section porosity and fatigue life graphics on figures 4.11-4.19 in order to get a general idea of what happens to those samples which have poor fatigue life. Starting by figure 4.13, a porosity ratio of 0.67% is found while measuring it using Archimedes method and a low porosity concentration is observed in cross-section image as well as a low quantity of defects on fracture surface although its fatigue life is under trend line. While for figure 4.17, a porosity ratio of 5.45% is found while measuring it using Archimedes method although a low porosity concentration is observed in cross-section image as well as a low quantity of defects on fracture surface. Both samples have in common that most of its porosity is located close to the fracture surface even though there is a low amount of defects detected on their fracture surface. Then, for samples built at 90 degrees, porosity is not concentrated close to the fracture surface even though those are the ones having the grater porosity ratio and those ones has a great amount of defects detected on their fracture

surface as seen on figures 4.18 and 4.19. This can indicate that porosity is in specific locations and might be a group of pores close to the fracture surface in the other half of the sample. Then, for samples built at 45 degrees, pores are concentrated close to the fracture surface although there is a low porosity ratio and almost all of these samples are on the fatigue life trend line.

Thus, a manufacturing failure can be occurring for samples built at 0 and 90 degrees since samples built at 45 degrees are from a different set of 3D-printed samples while samples built at 90 degrees are the ones which have the highest porosity ratio as well as the highest roughness values. It can also indicate that this geometry is not an optimal geometry for 3D metal printing at 0 and 90 degrees since samples have a tapered geometry which could cause an increment of porosity due to argon flow going into the melt pool as aforesaid.

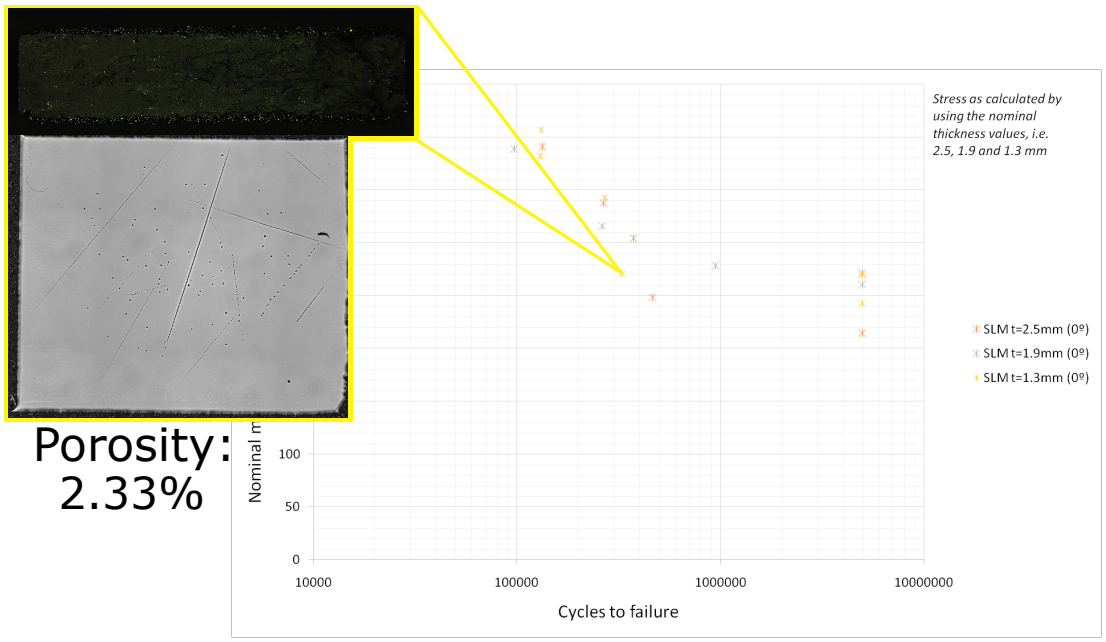

Figure 4.11: 1,3 mm thickness samples built at 0 degrees

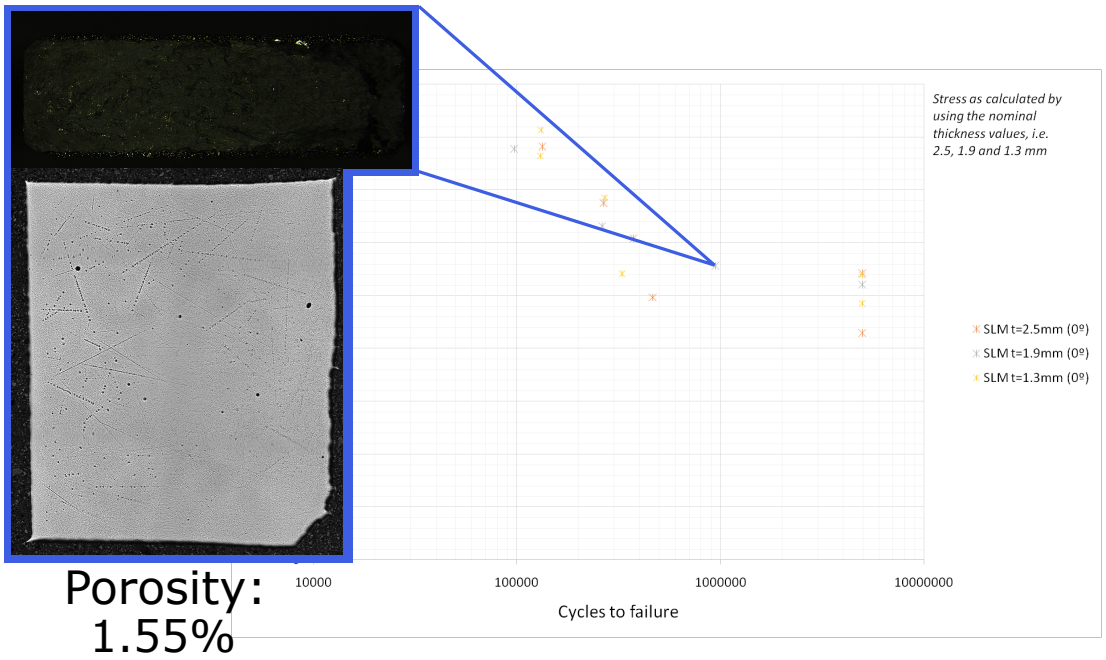

Figure 4.12: 1,9 mm thickness samples built at 0 degrees

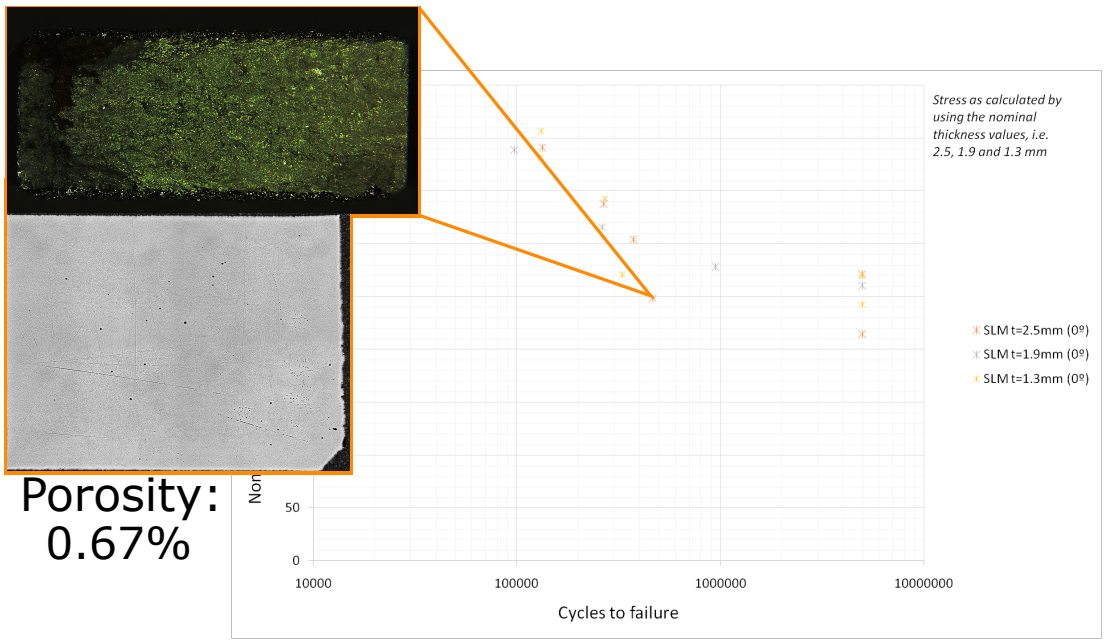

Figure 4.13: 2.5 mm thickness samples built at 0 degrees

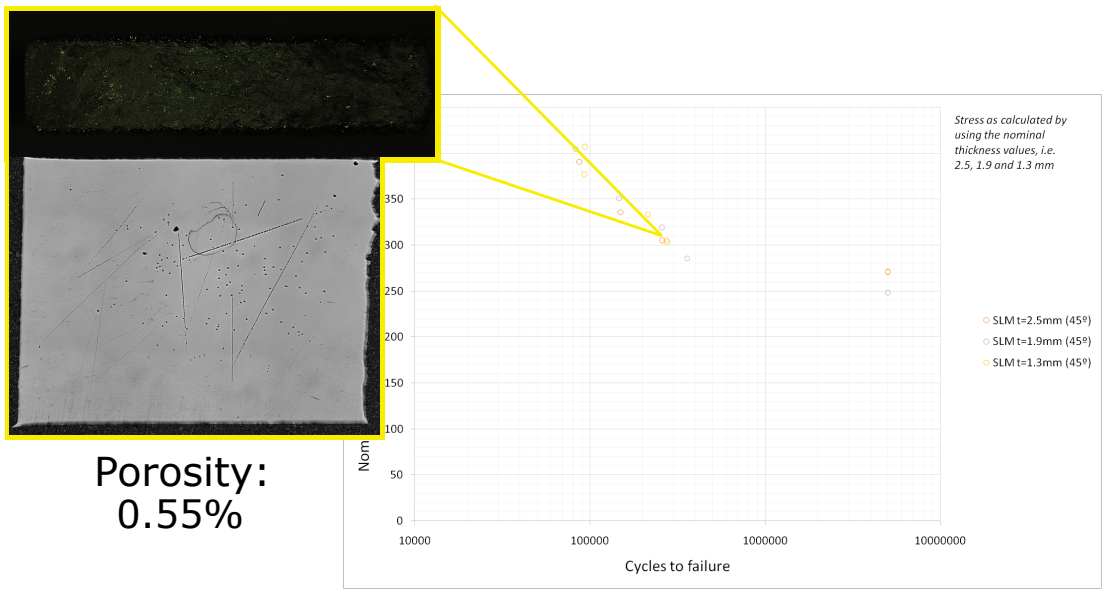

Figure 4.14: 1,3 mm thickness samples built at 45 degrees

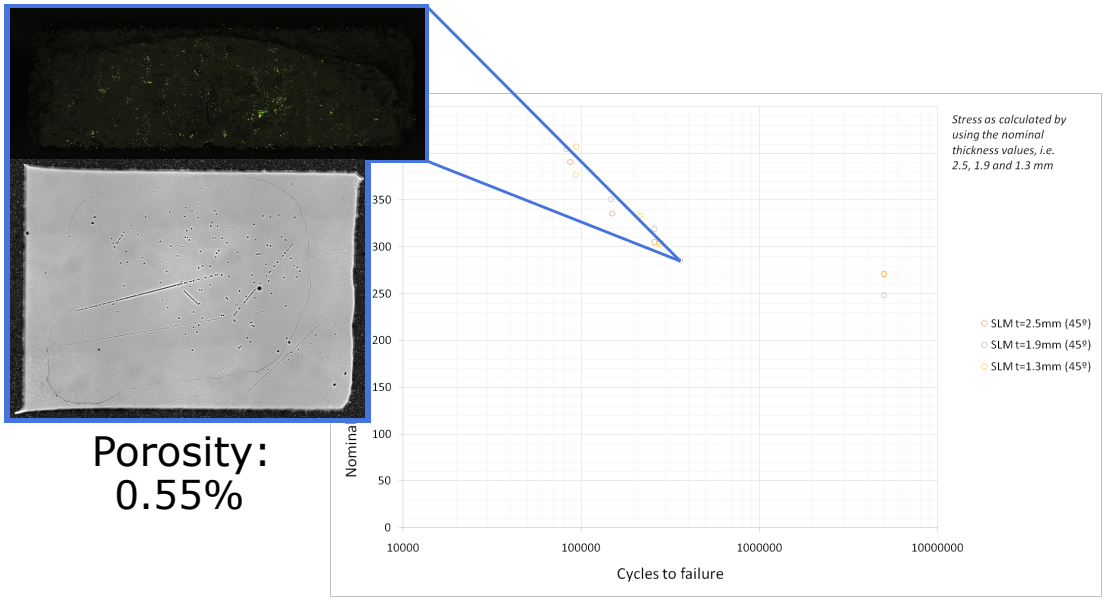

Figure 4.15: 1,9 mm thickness samples built at 45 degrees

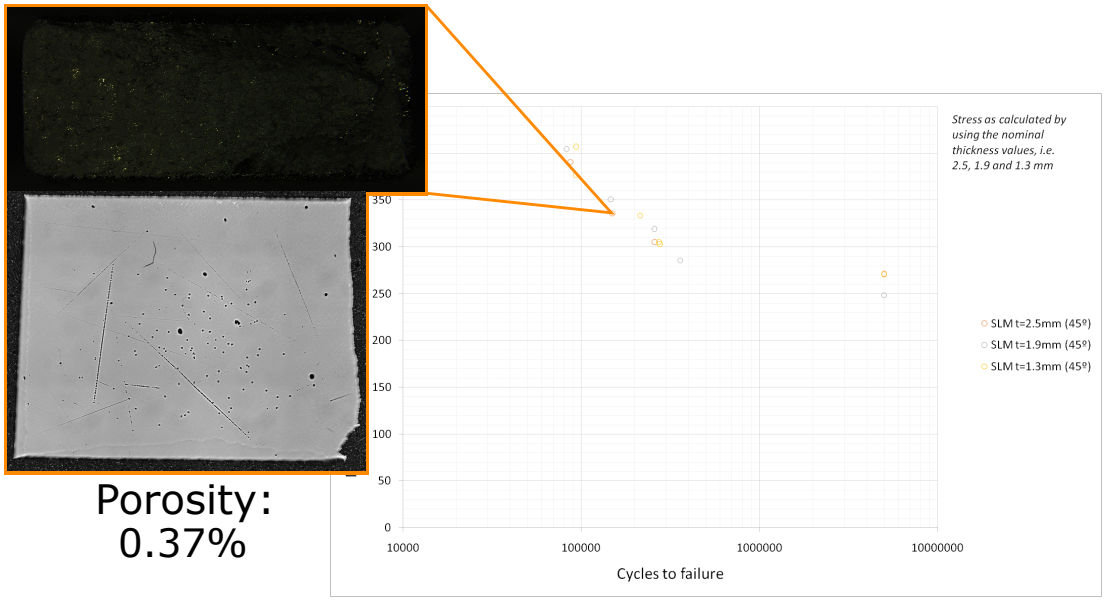

Figure 4.16: 2.5 mm thickness samples built at 45 degrees

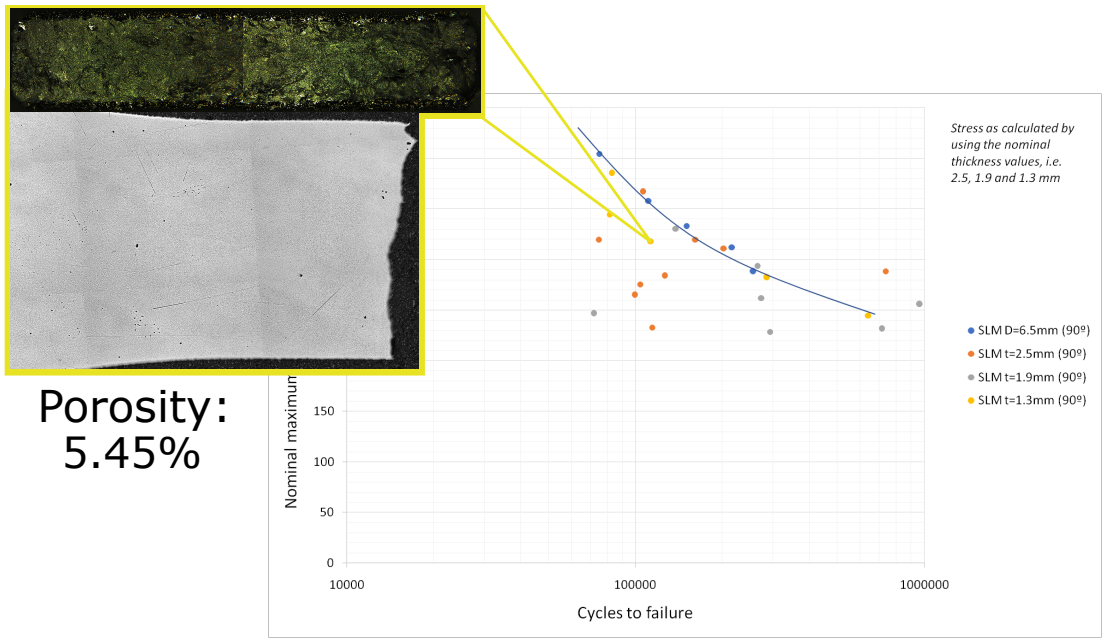

Figure 4.17: 1,3 mm thickness samples built at 90 degrees

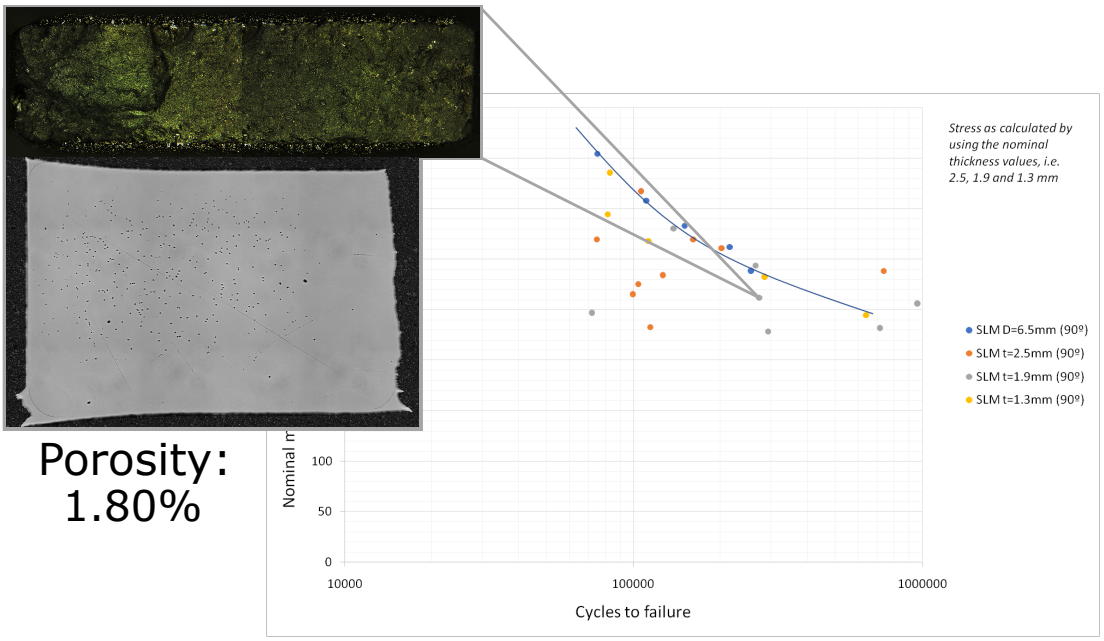

Figure 4.18: 1,9 mm thickness samples built at 90 degrees

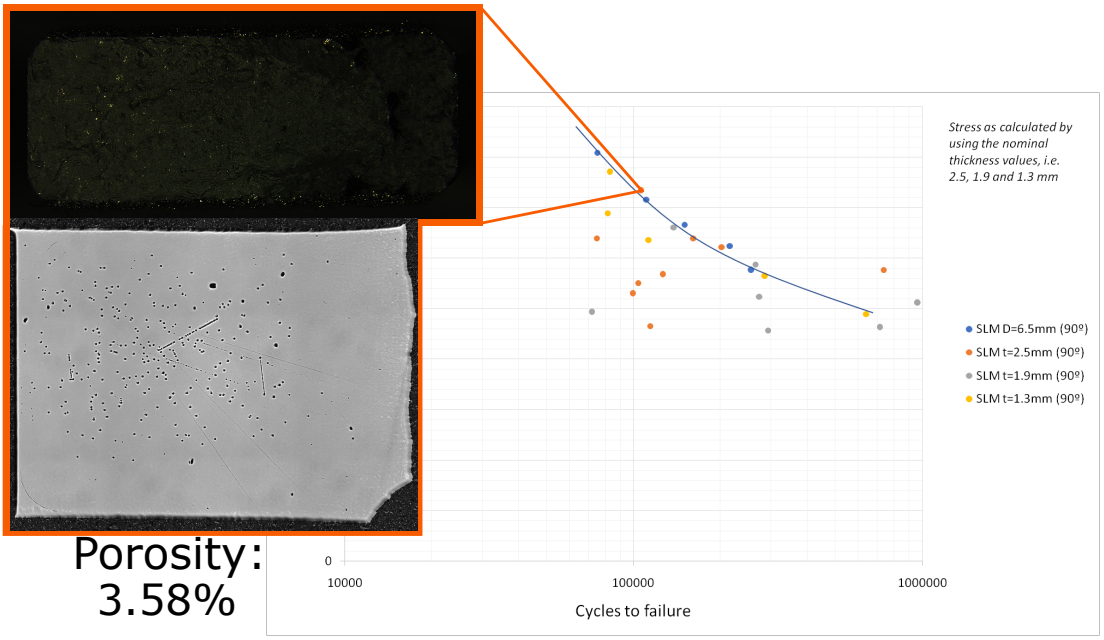

Figure 4.19: 2.5 mm thickness samples built at 90 degrees

5 Conclusions

This research aimed to identify why some samples tested in previous work had a poor fatigue life generating a scatter in fatigue graphics as aforesaid. Based on a quantitative and qualitative analysis of surface defects as well as internal defects such surface roughness and porosity, a conclusion about where the main problem resides is reached.

To begin with, results on surface roughness indicates that a general compensation factor values for all samples might not be used since a reduction of 47% is observed between samples built at 45 degrees (81.04 μm) and the current compensation factor value (150 μm), a reduction of 40% is observed between samples built at 0 degrees (92.08 μm) and the current compensation value (150 μm) and a reduction of 19% is observed between samples built at 90 degrees (123.56 μm) and the current compensation value (150 μm). Then, a value of 103 μm should be used instead of 150 μm if a general compensation factor values for all samples would be used. Otherwise, it would be more precise using each compensation factor for each sample building type so a better estimation of fatigue stress value will be obtained.

On the other hand, results on porosity measurements indicates that this defect has a considerable influence on fatigue test scatter since a porosity ratio of 2.39% is found for samples which are under fatigue life trend line, being this value higher than percentile value. However, a low defects degree is found on those samples' fracture surface although a cross-section reveals that a high pores concentration is found close to that fracture surface. This high porosity ratio due to lack of fusion and entrapped gas bubbles is likely to be the scatter on fatigue graphics main reason engendered owing to a poor fatigue life. Besides this, that great amount of pores helps to crack propagation shortening samples' fatigue life.

Finally, based on these conclusions, forthcoming research should consider manufacture all samples in different sets as if this will reduce manufacturing failures since those failures could be detected from one set to another and it can be corrected before next set is built.

REFERENCES

[1] Shifeng W, Shuai L, Qingsong W, Yan C, Sheng Z and Yusheng S. Effect of molten pool boundaries on the mechanical properties of selective laser melting parts. *Journal of Materials Processing Technology*, vol. 214, no. 11, pp. 2660–2667, 2014.

[2] Campbell F C. *Elements of metallurgy and engineering alloys*. ASM International, Materials Park Ohio, 2008.

[3] Jeon T, Hwang T, Yun H, VanTyne C and Moon Y. Control of porosity in parts produced by a direct laser melting process. *Applied Sciences*, vol. 8, no. 12, p. 2573, 2018.

[4] Gong H, Rafi K, Gu H, Starr T and Stucker B. Analysis of defect generation in ti–6al–4v parts made using powder bed fusion additive manufacturing processes. *Additive Manufacturing*, vol. 1-4, pp. 87–98, 2014.

[5] Ahsan M M. 3d printing and titanium alloys: A paper review md manjurul ahsan. *European Academic Research*, vol. 3, 2016.

[6] Bandyopadhyay A and Bose S. *Additive Manufacturing*. CRC Press, 2015.

[7] Duda T and Raghavan L V. 3d metal printing technology. *IFAC-PapersOnLine*, vol. 49, no. 29, pp. 103–110, 2016.

[8] Bandyopadhyay A and Bose S. *Additive Manufacturing*. CRC Press, 2015.

[9] Shougat M R E U, Sabuz E H, Quader G and Mahboob M. Effect of building orientation post processing material on mechanical properties of 3d printed parts. 2016.

[10] Guan K, Wang Z, Gao M, Li X and Zeng X. Effects of processing parameters on tensile properties of selective laser melted 304 stainless steel. *Materials & Design*, vol. 50, pp. 581–586, 2013.

[11] Hanzl P, Zetek M, Bakša T and Kroupa T. The influence of processing parameters on the mechanical properties of slm parts. *Procedia Engineering*, vol. 100, pp. 1405–1413, 2015.